Q. J. R. Meteorol. Soc. (1999), **125**, pp. 1445–1468

Cascade interpolation for semi-Lagrangian advection over the sphere

By RAMACHANDRAN NAIR, JEAN CÔTÉ and ANDREW STANIFORTH*
Meteorological Research Branch, Environment Canada

(Received 3 December 1997; revised 15 September 1998)

SUMMARY

A cascade interpolator, previously proposed by the authors for semi-Lagrangian advection in Cartesian geometry, is extended to spherical geometry. It is evaluated using two test problems—solid-body rotation and strong deformational flow—and found to be both accurate and efficient. The second problem is particularly challenging. It is a generalization to spherical geometry of Doswell's idealized cyclogenesis problem with an exact solution.

KEYWORDS: Cascade interpolation Idealized cyclogenesis Semi-Lagrangian advection Spherical domain

1. INTRODUCTION

Cascade interpolation employs a sequence of one-dimensional (1-D) interpolations to perform high-order interpolation in multi-dimensions in the context of semi-Lagrangian advection, and was first proposed by Purser and Leslie (1991), hereinafter referred to as PL91. These authors have subsequently demonstrated its effectiveness in a series of papers (Purser and Leslie 1994, 1996a,b, 1997; Leslie and Purser 1995) for both backward- and forward-trajectory semi-Lagrangian schemes: conventional interpolation techniques are particularly difficult and expensive for the latter. A typical tensor product interpolation in 3-D, based on the classical 1-D Lagrange interpolator, requires $O(p^3)$ operations per grid point per field, where p is the formal order of accuracy of the interpolator. However, a cascade scheme based on the same 1-D interpolator needs only $O(p)$ operations, a potentially significant saving. This, as advocated in the Purser and Leslie series of papers referred to above, makes the use of higher-order interpolation economically viable. There is, however, a non-negligible computational overhead incurred by the PL91 algorithm due to the cost of determining intersection points of the associated Eulerian and Lagrangian meshes.

Sun and Yeh (1997), hereinafter referred to as SY97, recently proposed a variant of cascade interpolation that also incorporates the monotonic filter introduced in Sun *et al.* (1996). This filter is based on that of Bermejo and Staniforth (1992), with a modification to better capture local extrema. Nair *et al.* (1999), hereinafter referred to as NCS99, significantly reduced the above-mentioned overhead of cascade interpolation by greatly simplifying the PL91 and SY97 procedures to determine mesh-intersection points, and demonstrated negligible loss of accuracy in the context of cubic interpolation. They also improved the robustness of the Sun *et al.* (1996) monotonic filter by eliminating spurious local minima that can occur in regions of large gradient.

Because of the economic promise of cascade interpolation, participants at a recent workshop sponsored by the European Centre for Medium-Range Weather Forecasts (ECMWF) recommended that it should be further developed for applications in spherical geometry (see European Centre for Medium-Range Weather Forecasts 1996). However, as noted in PL91, this is not straightforward due to the convergence of the meridians to the polar singularities of the spherical coordinate system. To address this issue, Purser and Leslie (1996b) introduced a variant of their cascade scheme that deforms the spherical mesh near the polar regions using a local mapping strategy. The procedure is

* Corresponding author, current affiliation: UK Meteorological Office, NWP Division, London Road, Bracknell, Berkshire RG12 2SZ, UK.

rather complex and computationally expensive, but this is somewhat mitigated by only being required within a spherical cap enclosing a given pole.

The purpose of the present work is to extend to spherical geometry (see section 2) the accurate and efficient NCS99 algorithm for Cartesian geometry. The extended scheme is evaluated in section 3 for a standard solid-body-rotation test problem, and in section 4 for a new test problem. This latter problem is a generalization to spherical geometry of Doswell's idealized cyclogenesis problem in Cartesian geometry, and it has an exact solution. Conclusions are given in section 5.

2. CASCADE INTERPOLATION ON A SPHERE

Consider the 2-D advection of a passive scalar ψ on a sphere:

$$\frac{\partial \psi}{\partial t} + \frac{u}{a \cos\theta} \frac{\partial \psi}{\partial \lambda} + \frac{v}{a} \frac{\partial \psi}{\partial \theta} = 0, \tag{1}$$

where λ and θ are respectively the longitude and latitude, u and v are the components of the velocity along the λ and θ directions, and a is the radius of the sphere. Let (λ_i, θ_j), where $i = 1, 2, \ldots, m$ and $j = 1, 2, \ldots, n$, define the regularly spaced Eulerian meshpoints, where uniform resolution ($\Delta\lambda$) is assumed in the λ direction, with m even. If the poles are meshpoints, then $\theta_1 \equiv -\pi/2$ and $\theta_n \equiv \pi/2$ respectively correspond to the south and north poles. The formulation thus includes uniform-resolution latitude–longitude meshes, with or without pole points, and the Gaussian grids of spectral models.

Assume that for every meshpoint (λ_i, θ_j) at time $t + \Delta t$ there exists a unique upstream Lagrangian point $(\lambda_{ij}, \theta_{ij})$ at time t, and that the position of this latter point is determined by integrating backwards in the usual way along a trajectory of the flow. Let (Λ, Θ) denote the curvilinear Lagrangian coordinate system corresponding to the Eulerian (λ, θ) system (Fig. 1). A θ-circle of the regular Eulerian mesh is a longitude circle, defined by $\lambda = \lambda_i$ and its continuation $\lambda = \lambda_{i+m/2} \equiv \lambda_i + \pi$. The associated Lagrangian Θ_i-curve, corresponding to the mapping of this θ_i-circle, is simply a deformed circle that joins the upstream points $(\lambda_{i1}, \theta_{i1}), (\lambda_{i2}, \theta_{i2}), \ldots, (\lambda_{in}, \theta_{in}), (\lambda_{i+m/2,n}, \theta_{i+m/2,n}), (\lambda_{i+m/2,n-1}, \theta_{i+m/2,n-1}), \ldots, (\lambda_{i+m/2,1}, \theta_{i+m/2,1})$. There are only $m/2$ such closed curves Θ_i, $i = 1, 2, \ldots, m/2$, due to the convention adopted here of 'wrapping a longitude around the whole globe' to simplify the cascade procedure in polar regions. Note that if the poles are meshpoints, then the south and north poles (λ_i, θ_1) and (λ_i, θ_n), where i is arbitrary, respectively map to the points $(\lambda_{i1}, \theta_{i1})$ and $(\lambda_{in}, \theta_{in})$ which are common to all Θ_i-curves. Also, the continuity and uniqueness of ψ at the south pole then imposes the constraints

$$\psi(\lambda_1, \theta_1) = \psi(\lambda_2, \theta_1) = \cdots = \psi(\lambda_m, \theta_1), \tag{2}$$

$$\psi(\lambda_{1,1}, \theta_{1,1}) = \psi(\lambda_{2,1}, \theta_{2,1}) = \cdots = \psi(\lambda_{m,1}, \theta_{m,1}), \tag{3}$$

and similarly for the north pole.

When the poles are meshpoints, the upstream values at the corresponding Lagrangian poles can be determined by interpolating along any or all of the Θ_i-curves, of which there are $m/2$. In the present work, the average of these $m/2$ values has been used. However, it was found that the results were virtually unchanged when making an arbitrary choice among the $m/2$ possible values, consistent with them only differing by truncation error.

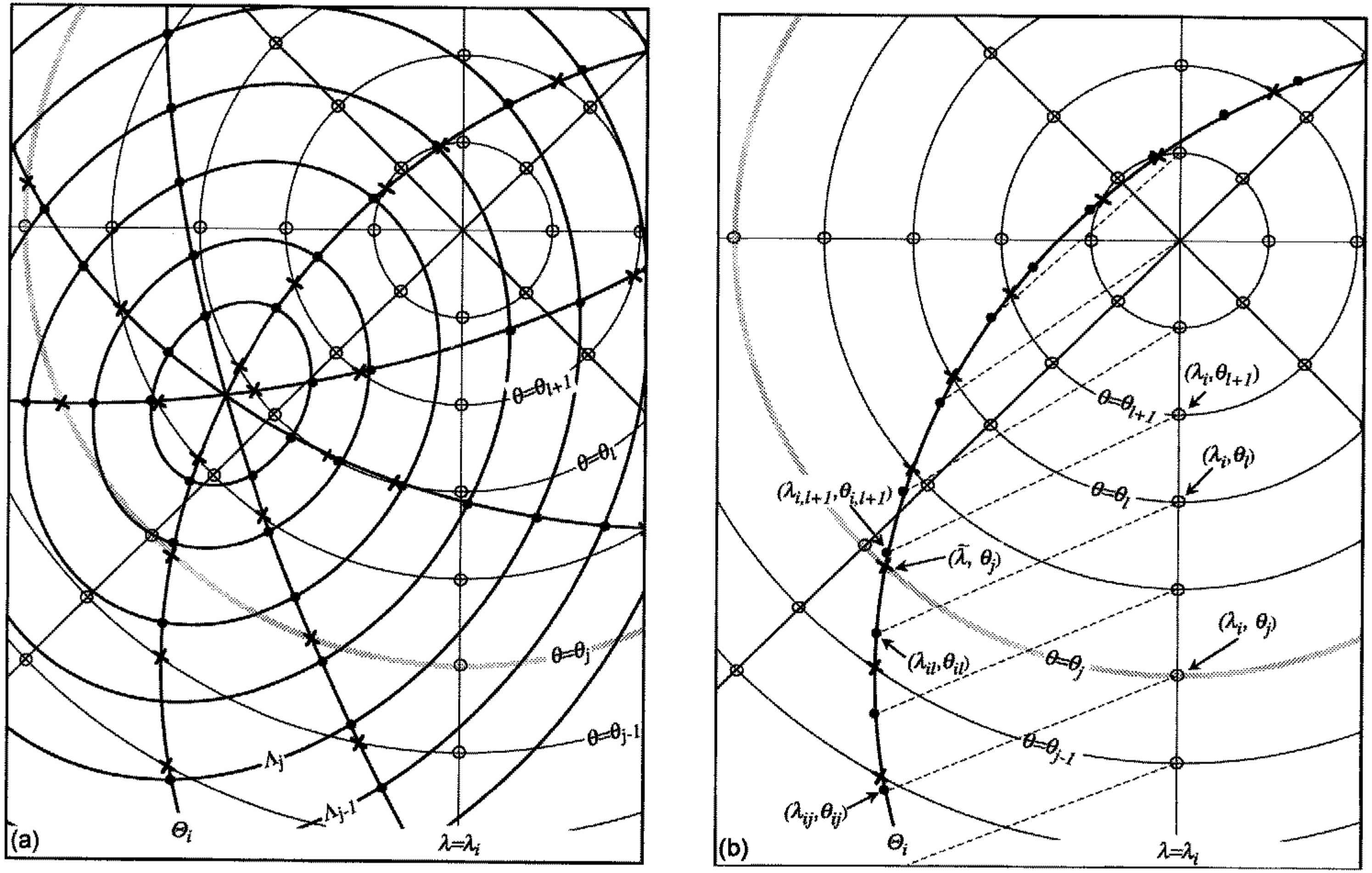

Figure 1. Schematics for cascade interpolation. Eulerian meshpoints are denoted by open circles, Lagrangian meshpoints by full circles, and intersection meshpoints by crosses. The standard Eulerian λ-line defined by $\theta = \theta_j$ is shown in grey. (a) Lagrangian (thick lines) and Eulerian (thin lines) meshes. (b) A specific Lagrangian Θ-curve Θ_i (also shown in (a)) that intersects θ_j at an intermediate meshpoint $\tilde{\lambda}$, θ_j; dashed lines denote backward trajectories.

(*a*) *Cascading the interpolation on a sphere*

The algorithm presented here for spherical geometry is a generalization of that given in NCS99 for Cartesian geometry. An intermediate mesh is defined by the intersection of the Lagrangian Θ_i-curves (i.e. $m/2$ deformed longitude circles) with the Eulerian λ-lines (i.e. n latitude circles defined by $\theta = \theta_j$). It can be summarized as:

(i) For $i = 1, 2, \ldots, m$ and $j = 1, 2, \ldots, n$; obtain in the usual way the upstream points $(\lambda_{ij}, \theta_{ij})$ that define the Lagrangian mesh.

(ii) Determine (see later) the location of the intersection points of Θ-curves (Lagrangian longitudes) with λ-circles (Eulerian latitudes).

(iii) For $j = 1, 2, \ldots, n$; interpolate, using 1-D polynomial interpolation along the λ-circles $\theta = \theta_j$, all advected fields from the meshpoints of the Eulerian mesh to the intersection meshpoints.

(iv) For $j = 1, 2, \ldots, n$; interpolate (see later), using 1-D polynomial interpolation along the Θ_i-curves (there are $m/2$ of them), all advected fields from the intersection meshpoints to the meshpoints of the Lagrangian mesh.

The 1-D interpolations can again be applied with or without monotonicity constraints. Periodic cubic-spline and cubic-Lagrange interpolators are used in the present study, but other choices are possible. It remains to specify how to determine the location of the meshpoints of the intermediate mesh, and how to subsequently interpolate along Lagrangian longitudes (i.e. Θ-curves).

(*b*) *Determination of the mesh intersection points*

Consider (Fig. 1(b)) a specific Θ_i-curve. If it intersects the specific Eulerian latitude circle $\theta = \theta_j$, then it will in general do so such that $\theta_{i\ell} \le \theta_j \le \theta_{i,\ell+1}$ for some value of the integer index ℓ, where $1 \le \ell \le n - 1$. It is natural to piecewise approximate the Θ_i-curve by great-circle segments since it is a deformed mapping of the great circle $\lambda = \lambda_i$. The intersection of the latitude circle with the segment of the great circle that joins the two points $(\lambda_{i\ell}, \theta_{i\ell})$ and $(\lambda_{i,\ell+1}, \theta_{i,\ell+1})$ of the Lagrangian mesh thus defines a point $(\tilde{\lambda}, \theta_j)$ of the intermediate mesh. It is convenient to perform the mesh navigation using a unit sphere ($a = 1$) and the Cartesian coordinates

$$\left.\begin{aligned} x &= \cos\lambda \cos\theta \\ y &= \sin\lambda \cos\theta \\ z &= \sin\theta \end{aligned}\right\} \Rightarrow x^2 + y^2 + z^2 = 1. \tag{4}$$

The equation of the θ_j-latitude circle is

$$x^2 + y^2 = \cos^2\theta_j. \tag{5}$$

Also, the great-circle plane that passes through the two points $(\lambda_{i\ell}, \theta_{i\ell})$ and $(\lambda_{i,\ell+1}, \theta_{i,\ell+1})$ is given by

$$A\,x + B\,y + C\,z = 0, \tag{6}$$

where

$$(A, B, C) = (x_{i\ell}, y_{i\ell}, z_{i\ell}) \times (x_{i,\ell+1}, y_{i,\ell+1}, z_{i,\ell+1}), \tag{7}$$

and $(x_{i\ell}, y_{i\ell}, z_{i\ell})$ and $(x_{i,\ell+1}, y_{i,\ell+1}, z_{i,\ell+1})$ are obtained by respectively evaluating (4) at the latitude–longitude points $(\lambda_{i\ell}, \theta_{i\ell})$ and $(\lambda_{i,\ell+1}, \theta_{i,\ell+1})$. The intersection of this

plane with the latitude plane $\theta = \theta_j$ is therefore the straight line

$$A\,x + B\,y = -C \sin\theta_j. \tag{8}$$

The coordinates of the intersection point of this line and the θ_j-latitude circle may now be found by simultaneously solving (5) and (8). This leads to the quadratic equation

$$(A^2 + B^2)x^2 + (2\,A\,C\,\sin\theta_j)x + \{(B^2 + C^2)\sin^2\theta_j - B^2)\} = 0. \tag{9}$$

The coordinates $(\tilde{\lambda}, \theta_j)$ of the sought intersection point are then found by solving (9) for x, and the corresponding y is given by (8). The value of $\tilde{\lambda}$ follows from

$$\tilde{\lambda} = \tan^{-1}(y/x), \tag{10}$$

where the inverse tangent is computed by first using the Fortran intrinsic function ATAN2, and then adding 2π to the result if it is in the interval $[-\pi, 0)$ to locate the root(s) in $[0, 2\pi)$. The quadratic equation (9) gives two values for x, and hence two values for $\tilde{\lambda}$: a procedure to select the right root is given in the next section. The set of all such points $(\tilde{\lambda}, \theta_j)$ defines the mesh intersection points used for the cascade interpolation.

There are other ways, possibly more efficient depending upon computer architecture, of determining the mesh-intersection points than that described here. For example, strictly speaking and at the expense of introducing some additional logic, it is only necessary to find one of the roots of (9) and thereby one value of $\tilde{\lambda}$, since the other value can be obtained by simply phase shifting $\tilde{\lambda}$ by π. Also, a very good first guess for a rapidly converging iterative procedure can be obtained by finding the intersection point of the latitude plane $\theta = \theta_j$ with the chord joining together the points $(\lambda_{i\ell}, \theta_{i\ell})$ and $(\lambda_{i,\ell+1}, \theta_{i,\ell+1})$.

(c) *Interpolation along the Lagrangian longitudes* Θ_i

Recall that the Θ_i-curve is defined by joining (Fig. 1) the points $(\lambda_{i1}, \theta_{i1})$, $(\lambda_{i2}, \theta_{i2})$, $\ldots$, $(\lambda_{in}, \theta_{in})$, $(\lambda_{i+m/2,n}, \theta_{i+m/2,n})$, $(\lambda_{i+m/2,n-1}, \theta_{i+m/2,n-1})$, $\ldots$, $(\lambda_{i+m/2,1}, \theta_{i+m/2,1})$ together along great-circle segments in a piecewise manner. The interpolation along Lagrangian latitudes Θ_i is performed using the distance s along the curve (normalized to the unit sphere) as independent variable.

The incremental distance $\Delta s_{i\ell}$ along the great-circle segment joining together two points $(\lambda_{i\ell}, \theta_{i\ell})$ and $(\lambda_{i,\ell+1}, \theta_{i,\ell+1})$ of the Θ_i-curve, obtained using the dot product of the two position vectors from the origin, is

$$\Delta s_{i\ell} = \cos^{-1}(x_{i\ell}x_{i,\ell+1} + y_{i\ell}y_{i,\ell+1} + z_{i\ell}z_{i,\ell+1}), \tag{11}$$

where the principal value is to be taken. The total distance along the curve from the reference point $(\lambda_{i,1}, \theta_{i,1})$ is then obtained by a summation of these incremental distances. A point $(\tilde{\lambda}, \theta_j)$ of the intermediate mesh lying on the great-circle segment joining the two Lagrangian points $(\lambda_{i\ell}, \theta_{i\ell})$ to $(\lambda_{i,\ell+1}, \theta_{i,\ell+1})$ lies at a distance

$$\Delta\tilde{s} = \cos^{-1}(x_{i\ell}\tilde{x} + y_{i\ell}\tilde{y} + z_{i\ell}\tilde{z}) \tag{12}$$

(principal value), from the Lagrangian point $(\lambda_{i\ell}, \theta_{i\ell})$. Of the two possible values for $\tilde{\lambda}$, the correct value satisfies

$$\Delta\tilde{s} \leq \Delta s_{i\ell}. \tag{13}$$

Now that the (non-uniform) relative position of all the points along the piecewise-defined Lagrangian latitudes Θ_i is known, the periodic interpolation to the upstream departure points $(\lambda_{ij}, \theta_{ij})$ proceeds in the usual manner (cf. NCS99).

3. SOLID-BODY ROTATION

To test the proposed cascade interpolation schemes in spherical geometry, a series of tests are presented for semi-Lagrangian advection using backward trajectories. The first of these is for solid-body rotation of a cosine bell. This problem is widely used to test advection schemes in spherical geometry (Ritchie 1987; Williamson and Rasch 1989; Rasch 1994; Li and Chang 1996; Lin and Rood 1996; McGregor 1996; Tolstykh 1996). Unfortunately, and despite the laudable effort of Williamson *et al.* (1992) to standardize problem definition and error measures in order to facilitate the intercomparison of results, experimental configurations and the manner of presenting results differ significantly in detail from study to study. The basis for the majority of experimental set-ups seems to be that introduced in Williamson and Rasch (1989) and it is the one adopted here.

(*a*) *Problem definition*

The velocity components of the advecting wind field are given by

$$u = u_0(\cos\alpha\cos\theta + \sin\alpha\cos\lambda\sin\theta), \tag{14}$$

$$v = -u_0\sin\alpha\sin\lambda, \tag{15}$$

where α is the angle between the axis of solid-body rotation and the polar axis of the spherical coordinate system (Williamson and Rasch 1989; Williamson *et al.* 1992). The flow field is such that when $\alpha = 0$ the axis of rotation is the polar axis, and when $\alpha = \pi/2$ it is in the equatorial plane. The initial scalar distribution is assumed to be a cosine bell. Thus

$$\psi(\lambda, \theta) = \begin{cases} \frac{1}{2}\{1 + \cos(\pi r/R)\}, & \text{if } r < R, \\ 0, & \text{if } r \geq R, \end{cases} \tag{16}$$

where

$$r = \cos^{-1}\{\sin\theta_c\sin\theta + \cos\theta_c\cos\theta\cos(\lambda - \lambda_c)\},$$

is the great-circle distance between (λ, θ) and the bell centre, initially taken as $(\lambda_c, \theta_c) = (3\pi/2, 0)$. The bell radius R is set to $7\pi/64$ as in Williamson and Rasch (1989), Rasch (1994), Li and Chang (1996), and Lin and Rood (1996), rather than to the value of 1/3 proposed in Williamson *et al.* (1992).

The computational domain consists of a 128×65 uniform-resolution (2.8125°) mesh where the first and last latitudinal grid lines represent the south and the north poles respectively. The time-step and the value of the maximum wind speed u_0 are chosen such that the angular velocity of the rotational flow is $\omega = 2\pi/256$ per time-step. Thus a complete revolution around the globe takes 256 time-steps, and the maximum Courant number is approximately 10.

(*b*) *Error measures*

The global measures of error in the numerical experiments are defined as in Williamson *et al.* (1992). They are:

$$l_1(\psi) = \frac{I(|\psi - \psi_T|)}{I(|\psi_T|)}, \tag{17}$$

$$l_2(\psi) = \frac{\left[I\{(\psi - \psi_T)^2\}\right]^{1/2}}{\left[I\{(\psi_T)^2\}\right]^{1/2}}, \tag{18}$$

$$l_\infty(\psi) = \frac{\max_{\forall \lambda,\theta} |\psi - \psi_T|}{\max_{\forall \lambda,\theta} |\psi_T|}, \tag{19}$$

$$M(\psi) = \frac{(\bar{\psi} - \bar{\psi}_T)}{\bar{\psi}_0}, \tag{20}$$

$$V(\psi) = \frac{I\left\{(\psi - \bar{\psi})^2\right\} - I\left\{(\psi_T - \bar{\psi}_T)^2\right\}}{I\left\{(\psi_0 - \bar{\psi}_0)^2\right\}}, \tag{21}$$

$$\psi_{\max} = \frac{\max_{\forall \lambda,\theta}(\psi) - \max_{\forall \lambda,\theta}(\psi_T)}{\Delta\psi_0}, \tag{22}$$

$$\psi_{\min} = \frac{\min_{\forall \lambda,\theta}(\psi) - \min_{\forall \lambda,\theta}(\psi_T)}{\Delta\psi_0}, \tag{23}$$

where $l_1(\psi)$, $l_2(\psi)$ and $l_\infty(\psi)$ are standard norms; $M(\psi)$, $V(\psi)$, $\psi_{\max}$ and $\psi_{\min}$ respectively are the normalized mean, variance, global maximum and global minimum of the field; ψ_T and ψ_0 are respectively the true solution and its initial value; $\Delta\psi_0 = \max_{\forall \lambda,\theta}(\psi_0) - \min_{\forall \lambda,\theta}(\psi_0)$ is the difference between the maximum and minimum values of the true solution initially; and I is the discrete approximation of the global integral

$$I(\psi) \equiv \bar{\psi} = \frac{1}{4\pi}\int_0^{2\pi}\int_{-\pi/2}^{\pi/2} \psi(\lambda, \theta)\cos\theta \, d\lambda \, d\theta. \tag{24}$$

(c) *Results*

Experiments have been performed for $\alpha = 0, \epsilon, \pi/2 - \epsilon$ and $\pi/2$ as recommended by Williamson *et al.* (1992), where $\epsilon = 0.05$ is the shift parameter. Trajectories are either evaluated exactly or approximately using the Côté and Staniforth (1988) algorithm with bilinear interpolation. In the discussion of results, attention is, however, focused on experiments that use exact trajectories, since cascade interpolation is then the sole source of error. Three different interpolators have been used, and these are denoted by: cascade cubic-spline; cascade cubic-Lagrange; and bicubic-Lagrange; and no monotonicity constraint is applied. The first two interpolators respectively correspond to using cubic-spline and cubic-Lagrange interpolation for the 1-D interpolator of the cascade algorithm described in section 2. The third interpolator is used to provide a reference result typical of those obtained using conventional bicubic interpolation in previous studies.

Results after one complete revolution around the globe (256 time-steps) using cascade cubic-spline interpolation and cascade cubic-Lagrange interpolation are respectively displayed in Figs. 2–3 as a function of α, together with the analytic solution. Figures 2(a)–(b) and 3(a)–(b) are for polar flow (i.e. the advection direction is poleward or near poleward, with the bell passing over the two poles during the course of the integration); Figs. 2(c)–(d) and 3(c)–(d) are for equatorial flow (i.e. the cosine bell is confined to an equatorial region).

From Fig. 2, all four results when using cascade cubic-spline interpolation are of generally similar accuracy, and this is confirmed by the error measures (see Table 1) at the end of the integration. Also, the bell has undergone a small stretching in the direction of the flow trajectories. A time sequence is shown in Fig. 4 for the offset polar flow (i.e. $\alpha = \pi/2 - \epsilon$) as the cosine bell approaches, passes over, and leaves the two polar regions. Such a flow field avoids the symmetry of the flow about the pole (Williamson

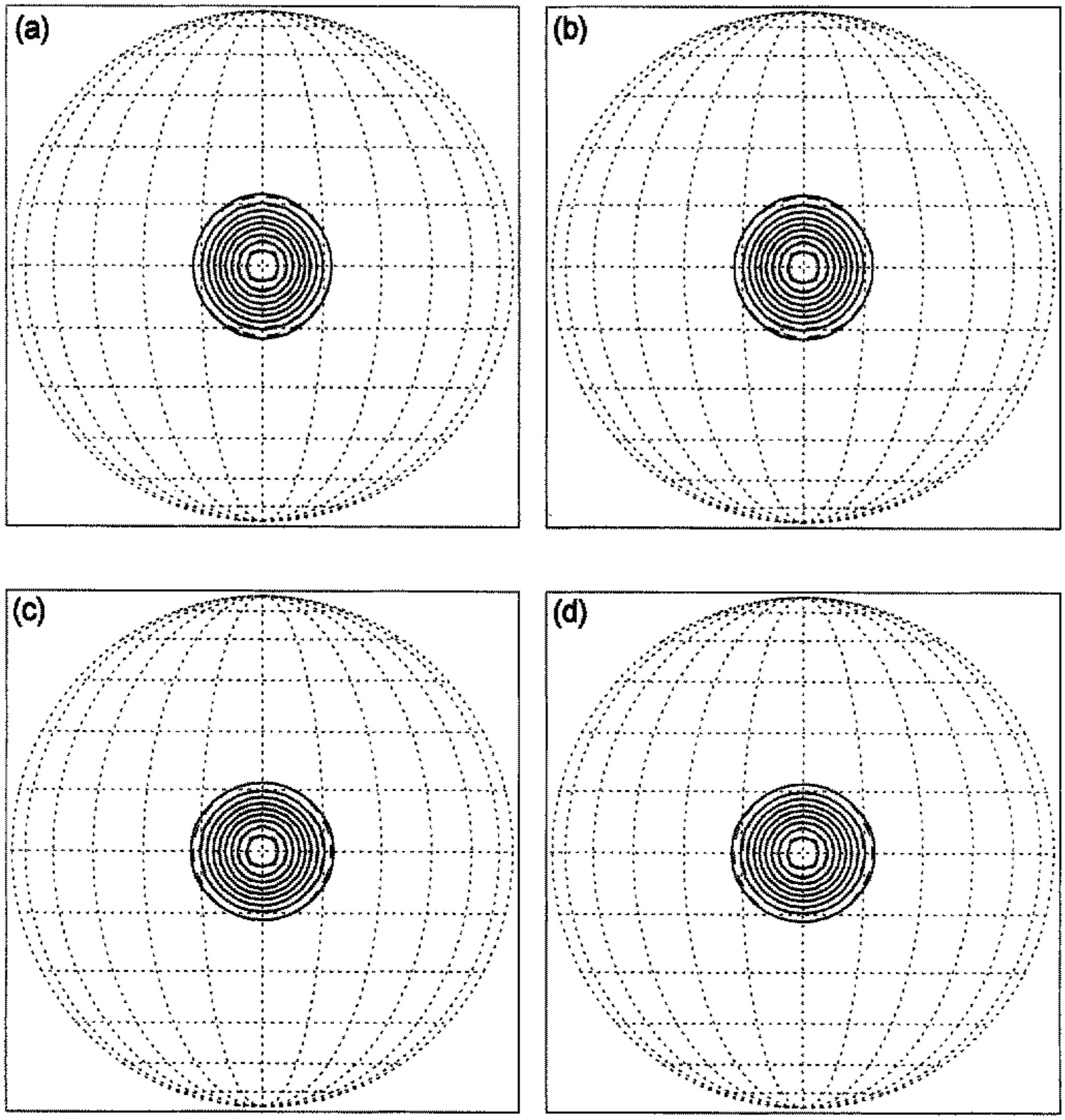

Figure 2. Results on an orthographic projection for solid-body rotation of a cosine bell after one revolution using cascade cubic-spline interpolation (solid contours). (a) Polar flow with $\alpha = \pi/2$ and (b) polar flow with $\alpha = \pi/2 - \epsilon$, where $\epsilon = 0.05$; (c) equatorial flow with $\alpha = 0$ and (d) equatorial flow with $\alpha = \epsilon$. The analytic solution is shown by dashed contours. See text for further explanation.

et al. 1992) and is a more stringent test than when $\alpha = \pi/2$. The convergence of the meridians has not resulted in a visible distortion of the cosine bell as it passes over the two poles.

From Fig. 3, using a 1-D cubic-Lagrange interpolator instead of a 1-D cubic-spline one in the cascade interpolation procedure results in a visible degradation of the results, primarily a stretching in the direction of the flow. This is confirmed by the error measures obtained at the end of the integration and given in Table 2. In particular the l_1, l_2 and l_∞ errors are all approximately four times larger for cascade cubic-Lagrange interpolation than for cascade cubic-spline interpolation. This is consistent with the finding of Makar and Karpik (1996) that bicubic-spline interpolation performs significantly better than bicubic-Lagrange interpolation in the context of solid-body rotation of a cone around a sphere. The time sequence in Fig. 5 for the offset polar flow (i.e. $\alpha = \pi/2 - \epsilon$)

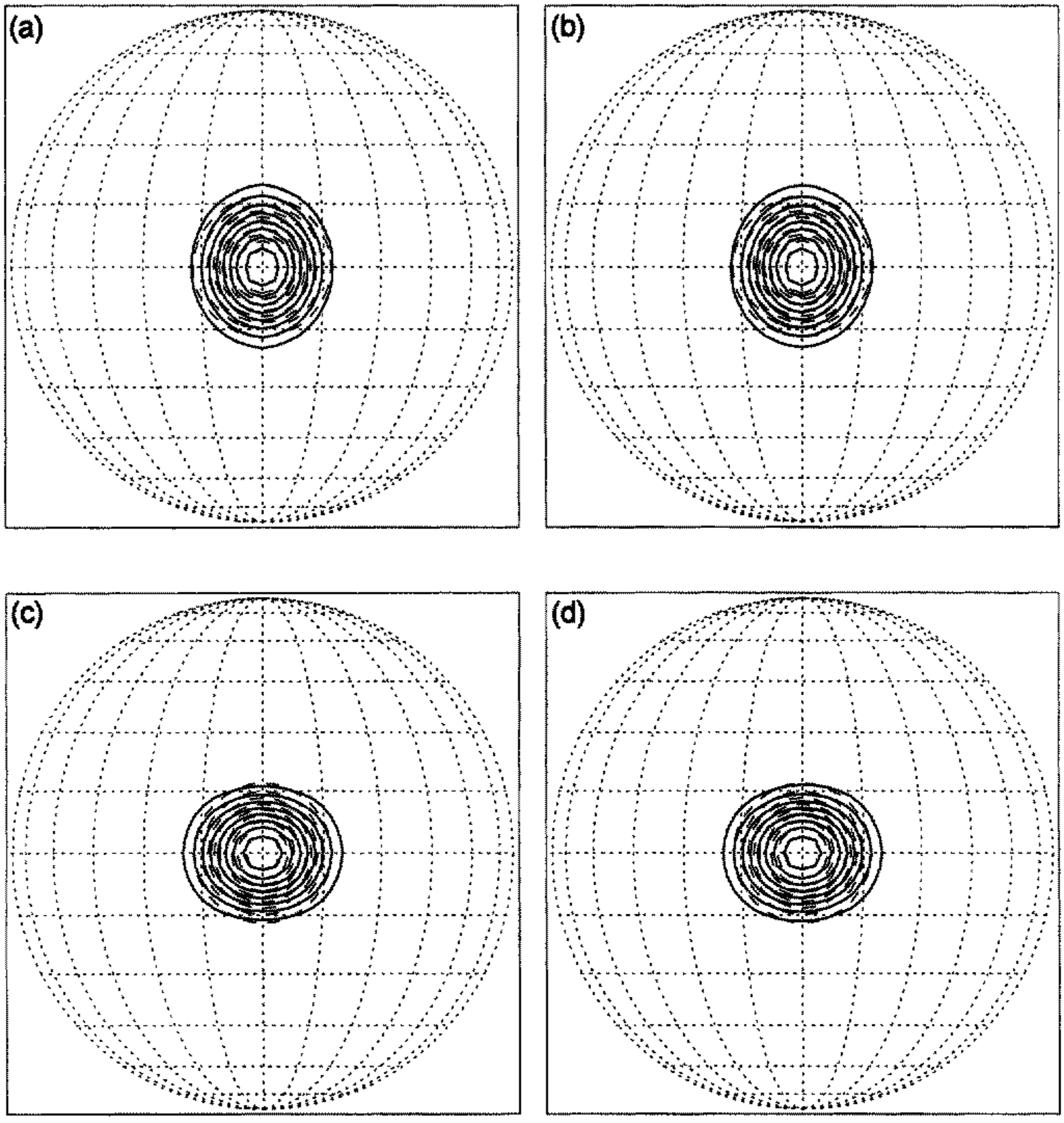

Figure 3. As in Fig. 2, but using cascade cubic-Lagrange interpolation.

TABLE 1. ERROR MEASURES (DEFINED IN TEXT), AS A FUNCTION OF ROTATION ANGLE α, FOR SOLID-BODY ROTATION OF A COSINE BELL AFTER ONE REVOLUTION USING A SEMI-LAGRANGIAN SCHEME WITH CASCADE CUBIC-SPLINE INTERPOLATION AND EXACT TRAJECTORIES: SHIFT PARAMETER $\epsilon = 0.05$

α	l_1	l_2	l_∞	M	V	$\psi_{\max}$	$\psi_{\min}$
0	0.0486	0.0334	0.0281	2.4×10^{-7}	−0.0197	−0.0135	−0.0153
ϵ	0.0491	0.0335	0.0279	-5.3×10^{-4}	−0.0208	−0.0153	−0.0153
$\pi/2 - \epsilon$	0.0495	0.0307	0.0290	3.0×10^{-4}	−0.0180	−0.0142	−0.0148
$\pi/2$	0.0506	0.0316	0.0354	4.8×10^{-4}	−0.0178	−0.0205	−0.0175

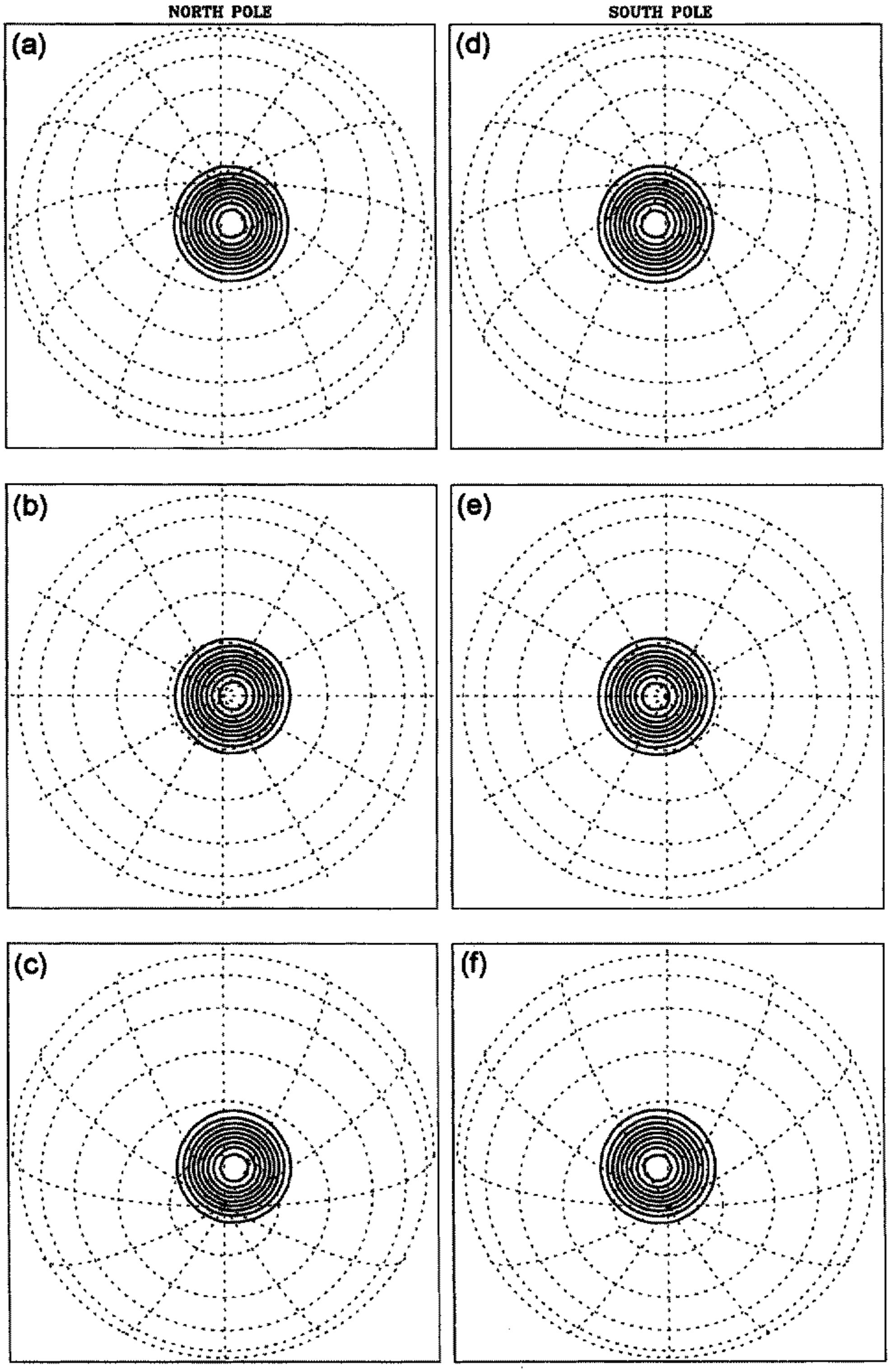

Figure 4. Results on an orthographic projection moving with the cosine bell for offset ($\alpha = \pi/2 - \epsilon$) solid-body rotation of a cosine bell: (a) approaching, (b) passing over, and (c) leaving the northern polar region at time-steps 56, 64 and 72, respectively; (d) approaching, (e) passing over, and (f) leaving the southern polar region at time-steps 184, 192 and 200, respectively.

TABLE 2. AS IN TABLE 1 BUT FOR CASCADE CUBIC-LAGRANGE INTERPOLATION

α	l_1	l_2	l_∞	M	V	ψ_{max}	ψ_{min}
0	0.215	0.148	0.109	4.8×10^{-7}	−0.108	−0.109	−0.0314
ϵ	0.220	0.149	0.116	-5.7×10^{-4}	−0.117	−0.116	−0.0308
$\pi/2 - \epsilon$	0.234	0.144	0.120	3.9×10^{-3}	−0.105	−0.120	−0.0296
$\pi/2$	0.235	0.144	0.121	6.7×10^{-3}	−0.099	−0.121	−0.0335

using cascade cubic-Lagrange interpolation shows that even though the flow is less-accurately represented than with cascade cubic-spline interpolation, there is again no visible distortion of the cosine bell as it passes over the two poles.

Results using bicubic-Lagrange interpolation, corresponding to those discussed above for the two cascade-interpolation schemes, are summarized in Table 3. Comparing Tables 1–3, bicubic-Lagrange interpolation leads to marginally better results than does cascade cubic-Lagrange interpolation, but both lead to substantially worse results than does cascade cubic-spline interpolation. Figures are not presented for integrations using bicubic-Lagrange interpolation since they are visually indistinguishable from the corresponding ones for cascade cubic-Lagrange interpolation.

TABLE 3. AS IN TABLE 1 BUT FOR BICUBIC-LAGRANGE INTERPOLATION

α	l_1	l_2	l_∞	M	V	ψ_{max}	ψ_{min}
0	0.215	0.148	0.109	1.2×10^{-7}	−0.108	−0.109	−0.0314
ϵ	0.215	0.148	0.110	-1.3×10^{-4}	−0.109	−0.110	−0.0310
$\pi/2 - \epsilon$	0.227	0.141	0.113	-1.7×10^{-3}	−0.100	−0.113	−0.0303
$\pi/2$	0.227	0.141	0.114	2.1×10^{-3}	−0.099	−0.114	−0.0310

The above set of experiments, obtained using exact trajectories, were repeated using trajectories computed by the Côté and Staniforth (1988) algorithm. This generally results in a negligible degradation of the results. For example, the errors summarized in Table 4 for experiments using cascade cubic-spline interpolation and computed trajectories are generally (but not always) slightly larger than the corresponding ones obtained using exact trajectories and given in Table 1.

The above-described results may be compared, albeit rather imperfectly due to variations in experimental configurations and incomplete information, with those of other studies. For equatorial flow (i.e. $\alpha = 0$) and semi-Lagrangian advection using bicubic-Lagrange interpolation, the errors given in Table 3, obtained using a 128×65 uniform latitude–longitude mesh and exact trajectories, are comparable to those given in Fig. 7(b) of McGregor (1996), obtained using a 128×64 Gaussian grid and computed trajectories. For poleward flow (i.e. $\alpha = \pi/2$), the above-described results may be compared with those obtained at similar resolution by Williamson and Rasch (1989),

TABLE 4. AS IN TABLE 1 BUT FOR TRAJECTORIES COMPUTED USING THE CÔTÉ AND STANIFORTH (1988) ALGORITHM

α	l_1	l_2	l_∞	M	V	ψ_{max}	ψ_{min}
0	0.0488	0.0334	0.0283	-4.2×10^{-4}	−0.0186	−0.0136	−0.0153
ϵ	0.0491	0.0335	0.0279	-2.2×10^{-4}	−0.0194	−0.0139	−0.0153
$\pi/2 - \epsilon$	0.0499	0.0309	0.0298	3.5×10^{-4}	−0.0180	−0.0142	−0.0148
$\pi/2$	0.0511	0.0319	0.0351	5.6×10^{-4}	−0.0178	−0.0205	−0.0175

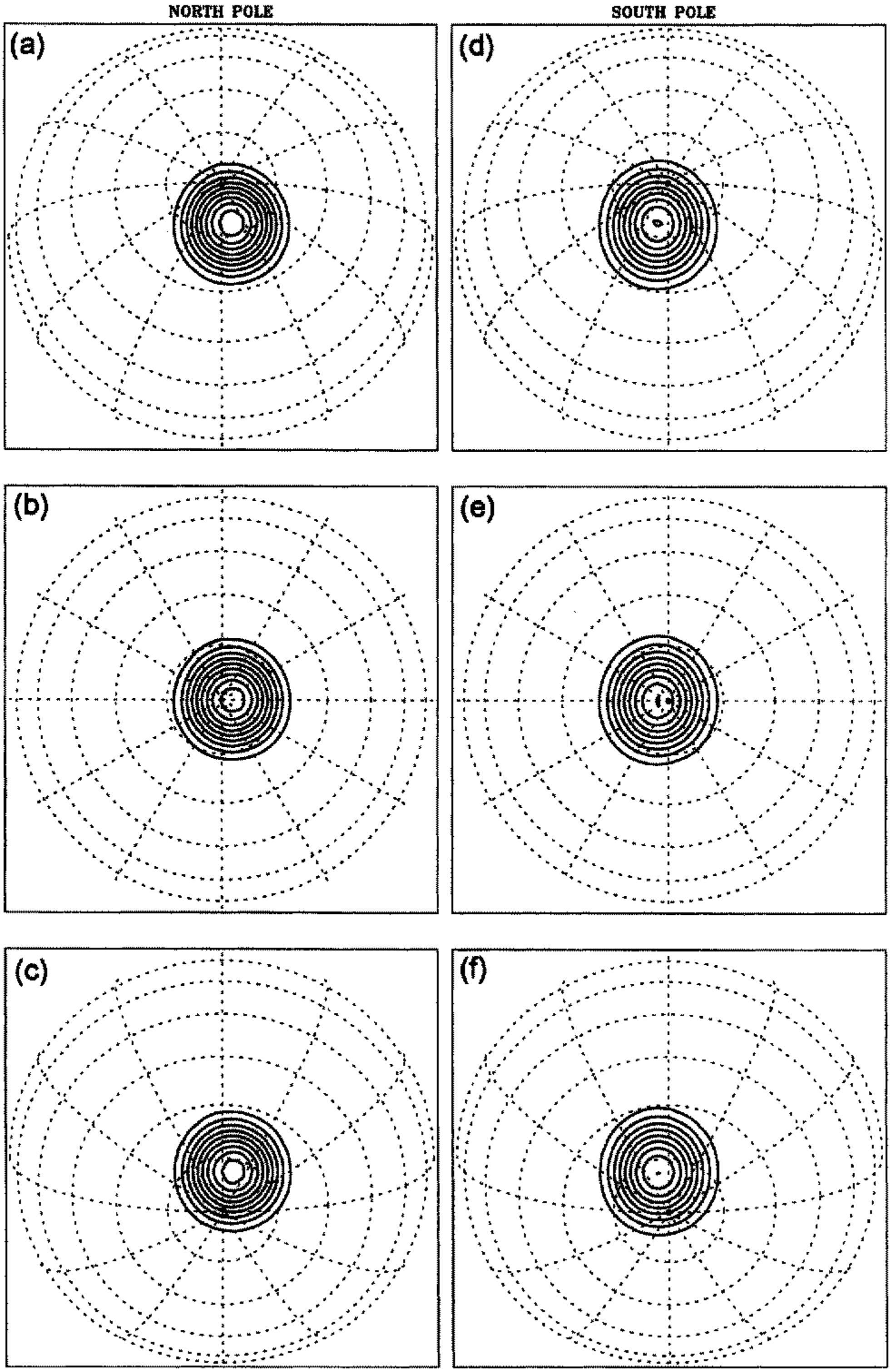

Figure 5. As in Fig. 4, but using cascade cubic-Lagrange interpolation.

TABLE 5. AS IN TABLE 1 BUT FOR POLAR FLOW ($\alpha = \pi/2$) USING VARIOUS PUBLISHED SCHEMES

Authors	Experiment	l_1	l_2	l_∞	M	V	ψ_{max}	ψ_{min}
Rasch	FG2.8	0.327	0.209	0.169	0	-8×10^{-4}	−0.152	−0.0411
Rasch	RG2.8	0.289	0.196	0.164	0	-8×10^{-4}	−0.150	−0.0271
Rasch	RG2.8M	0.181	0.158	0.196	0	-1×10^{-3}	−0.210	0
Li & Chang	Test 2	–	–	–	0	−0.031	−0.030	0
Li & Chang	Test 3	–	–	–	0	−0.022	−0.021	0
Lin & Rood	FFSL-3	0.078	0.079	0.124	0	–	−0.124	−0.0009
Lin & Rood	FFSL-5	0.047	0.041	0.053	0	–	−0.053	−0.0013

Rasch (1994), Li and Chang (1996), and Lin and Rood (1996). Available error measures are summarized for some of these in Table 5, where only the best schemes of each study have been selected, and can be compared with those displayed in Tables 1–4.

The cascade cubic-spline scheme generally appears to have smaller l_1, l_2 and l_∞ errors than do the other schemes, an exception being the FFSL-5 Lin and Rood (1996) scheme which has a somewhat smaller l_1 error (0.047 v 0.051) but larger l_2 (0.041 v 0.032) and l_∞ (0.053 v 0.035) errors. The Rasch (1994), Li and Chang (1996), and Lin and Rood (1996) schemes all formally conserve mass, and are therefore better in this respect than the schemes used here. The present schemes could be modified to impose conservation, e.g. as in Priestley (1993), at the price of some degradation of other error measures. This is not done here since the focus of the study is simply to describe and demonstrate an efficient way of performing cascade interpolation on the sphere, and not to compare and evaluate a plethora of advection schemes. Finally, the Rasch (1994) schemes have smaller variance errors but larger l_1, l_2 and l_∞ errors than those of the cited studies.

4. DEFORMATIONAL FLOW—IDEALIZED CYCLOGENESIS

The second test problem is an extension to spherical geometry of the idealized cyclogenesis problem of Doswell (1984) that has been used for scalar advection tests in Cartesian geometry by Rančić (1992), Hólm (1995), SY97 and NCS99. The flow field is deformational and more challenging than solid-body rotation.

(a) *Problem definition*

Let (λ', θ') be a rotated coordinate system with north pole at (λ_0, θ_0) with respect to the regular spherical coordinate system (λ, θ). A steady circular vortex is defined to have zero normal velocity $v' \equiv d\theta/dt$, and tangential velocity

$$u'(\theta') \equiv \cos\theta' \frac{d\lambda'}{dt} = \frac{3\sqrt{3}}{2} \operatorname{sech}^2(\gamma\rho) \tanh(\gamma\rho), \tag{25}$$

where

$$\rho(\theta') = \frac{2\cos\theta'}{1 + \sin\theta'}, \tag{26}$$

and γ is a (constant) stretching parameter that controls the length-scale of the vortex with respect to a unit sphere. Defining a polar-stereographic plane tangent to the north pole of the rotated coordinate system, the variable ρ can be interpreted (see appendix) as the distance from this pole of the projection of a point (λ', θ') onto this plane. The

amplitude of the vortex has been normalized to have a maximum tangential velocity of unity, and this occurs (see appendix) at

$$\theta' = 2 \tan^{-1} \left(\frac{\gamma - c}{\gamma + c} \right), \tag{27}$$

where

$$c = \frac{1}{4} \ln \left(\frac{\sqrt{3} + 1}{\sqrt{3} - 1} \right) \approx 0.3292395. \tag{28}$$

The initial condition for the advected scalar is $\psi(\lambda', \theta', 0) = -\tanh\{(\rho/\delta) \sin \lambda'\}$, where δ is the characteristic width of the frontal zone. Thus the analytic solution at time t is

$$\psi(\lambda', \theta', t) = -\tanh \left\{ \frac{\rho}{\delta} \sin(\lambda' - \omega t) \right\}, \tag{29}$$

where

$$\omega(\theta') = \frac{u'(\theta')}{\cos \theta'} \tag{30}$$

is angular velocity. The passive advection equation in the rotated coordinate system is given by (1), but with λ and θ respectively replaced by λ' and θ'. It is easily verified by substitution into the resulting equation that (29) is indeed an exact solution when the velocity field is specified by (25) and $v' = 0$.

Details are given in the appendix on the equivalent specification of this idealized cyclogenesis problem in the unrotated (λ, θ) coordinate system.

(*b*) *Results*

By setting $\gamma = 3/2$ and $\delta = 0.01$, and by integrating 2.5 time units on the same 128×65 uniform mesh defined in the previous section, a deformational advection problem in spherical geometry is obtained that is of similar numerical difficulty to that used in the SY97 and NCS99 studies in Cartesian geometry. This value for γ corresponds to centring the vortex at a latitude of approximately 65°N. Note that the isopleth of maximum wind speed passes over the north pole of the computational domain to strengthen the challenge for numerical advection schemes. The exact solution, after projection onto the plane tangent to the vortex center, is displayed in Fig. 6 at initial time and $t = 2.5$ time units.

The same global measures of error, defined by (17)–(23), are used here as those adopted in section 3 for solid-body rotation, but with one exception. The normalized mean M defined by (20) is singular for the present deformational problem. Since M is a measure of mass conservation, it is replaced by the mass measure used in NCS99 for the analogous deformational problem in Cartesian geometry, i.e. by the normalized quantity

$$Mass = \frac{I \left\{ \psi - \min_{\forall \lambda, \theta} (\psi_0) \right\}}{I \left\{ \psi_0 - \min_{\forall \lambda, \theta} (\psi_0) \right\}}. \tag{31}$$

This quantity has the value of unity when mass is exactly conserved.

Results at $t = 2.5$ are displayed in Figs. 7 and 8, without and with the use of the NCS99 filter, respectively, and summarized in Table 6. All were obtained using cascade

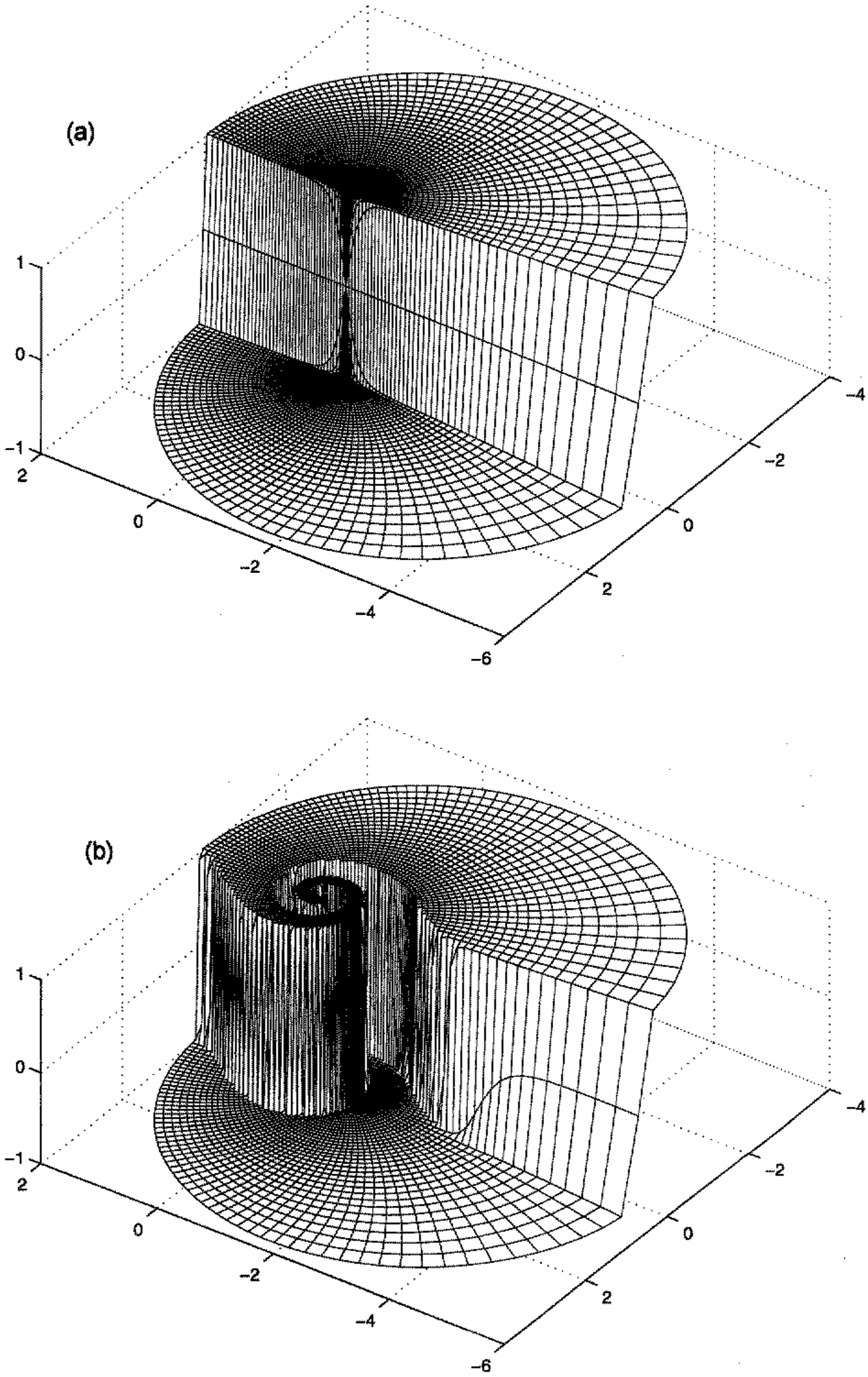

Figure 6. The exact solution (see text), projected onto the plane tangent to the vortex centre, at (a) initial time and (b) $t = 2.5$.

TABLE 6. ERROR MEASURES (DEFINED IN TEXT) AT $t = 2.5$ FOR DEFORMATIONAL FLOW, USING: A SEMI-LAGRANGIAN SCHEME WITH CASCADE CUBIC-SPLINE INTERPOLATION AND EXACT TRAJECTORIES; 16 OR 64 TIME-STEPS; AND WITHOUT OR WITH A MONOTONIC FILTER

Monotonic filter	No. of t-steps	l_1	l_2	l_∞	*Mass*	V	$\psi_{\max}$	$\psi_{\min}$
No	16	0.0297	0.0940	1.7440	1.0045	−0.0931	0.5684	−0.3111
No	64	0.0287	0.0843	1.0303	1.0039	−0.0963	0.1144	−0.1786
Yes	16	0.0283	0.0982	1.5260	1.0039	−0.1151	0	0
Yes	64	0.0302	0.0988	1.0571	1.0070	−0.1202	0	0

TABLE 7. AS IN TABLE 6, BUT FOR TRAJECTORIES COMPUTED USING THE CÔTÉ AND STANIFORTH (1988) ALGORITHM

Monotonic filter	No. of t-steps	l_1	l_2	l_∞	*Mass*	V	$\psi_{\max}$	$\psi_{\min}$
No	16	0.0309	0.1011	1.8660	1.0043	−0.0928	0.5335	−0.2878
No	64	0.0288	0.0849	1.0900	1.0040	−0.0962	0.1209	−0.1805
Yes	16	0.0295	0.1045	1.6338	1.0037	−0.1145	0	0
Yes	64	0.0301	0.0990	1.0492	1.0071	−0.1200	0	0

cubic-spline interpolation with exact trajectories and either 16 or 64 time-steps (which correspond to Courant numbers of approximately 64 and 16). An intercomparison of these results and the exact solution (Fig. 6(b)) reveals that: all four integrations generally represent the exact solution quite well; overshoots and undershoots are noticeable in the integrations without a monotonic filter (Fig.7), and particularly noticeable (Fig. 7(a)) for the longer time-step integration having fewer interpolations to damp the overshoots and undershoots of the Gibbs phenomenon; the monotonic NCS99 filter eliminates overshoots and undershoots (Fig. 8) while well maintaining the essential details of the exact solution; and the numerical solution is relatively insensitive to a quadrupling of time-step (cf. Figs. 7(a) and 8(a) with Figs. 7(b) and 8(b)) respectively. Note, however, that the normalized global maximum ($\psi_{\max}$) and minimum ($\psi_{\min}$), and the l_∞ norm, are quite large since they represent extreme values and are sensitive to the Gibbs phenomenon associated with the quasi-discontinuous nature of the solution. It has been verified, by plotting difference fields between the numerical results and the exact solution, that the larger errors all occur in the immediate vicinity of the quasi-discontinuity of the solution as expected.

The above set of experiments, obtained using exact trajectories, were repeated using trajectories computed by the Côté and Staniforth (1988) algorithm. The results are visually indistinguishable from those displayed in Figs. 7–8 and are therefore not shown. The error measures for this set of experiments are summarized in Table 7. Comparison of these with the corresponding ones (Table 6) obtained with exact trajectories confirms that the use of computed trajectories instead of exact ones has a marginal impact on the results.

A further set of experiments was performed, but this time using cascade cubic-Lagrange instead of cascade cubic-spline interpolation. On the one hand, this results in a less-severe Gibbs phenomenon in the absence of the monotonic NCS99 filter (cf. Figs. 7 and 9 respectively obtained using cascade cubic-spline and cascade cubic-Lagrange interpolation). On the other hand the results are visually indistinguishable from one another when the NCS99 filter is used, and are therefore not shown. Using cascade cubic-Lagrange instead of cascade cubic-spline interpolation worsens the l_1 and l_2 errors (cf. Tables 6 and 8).

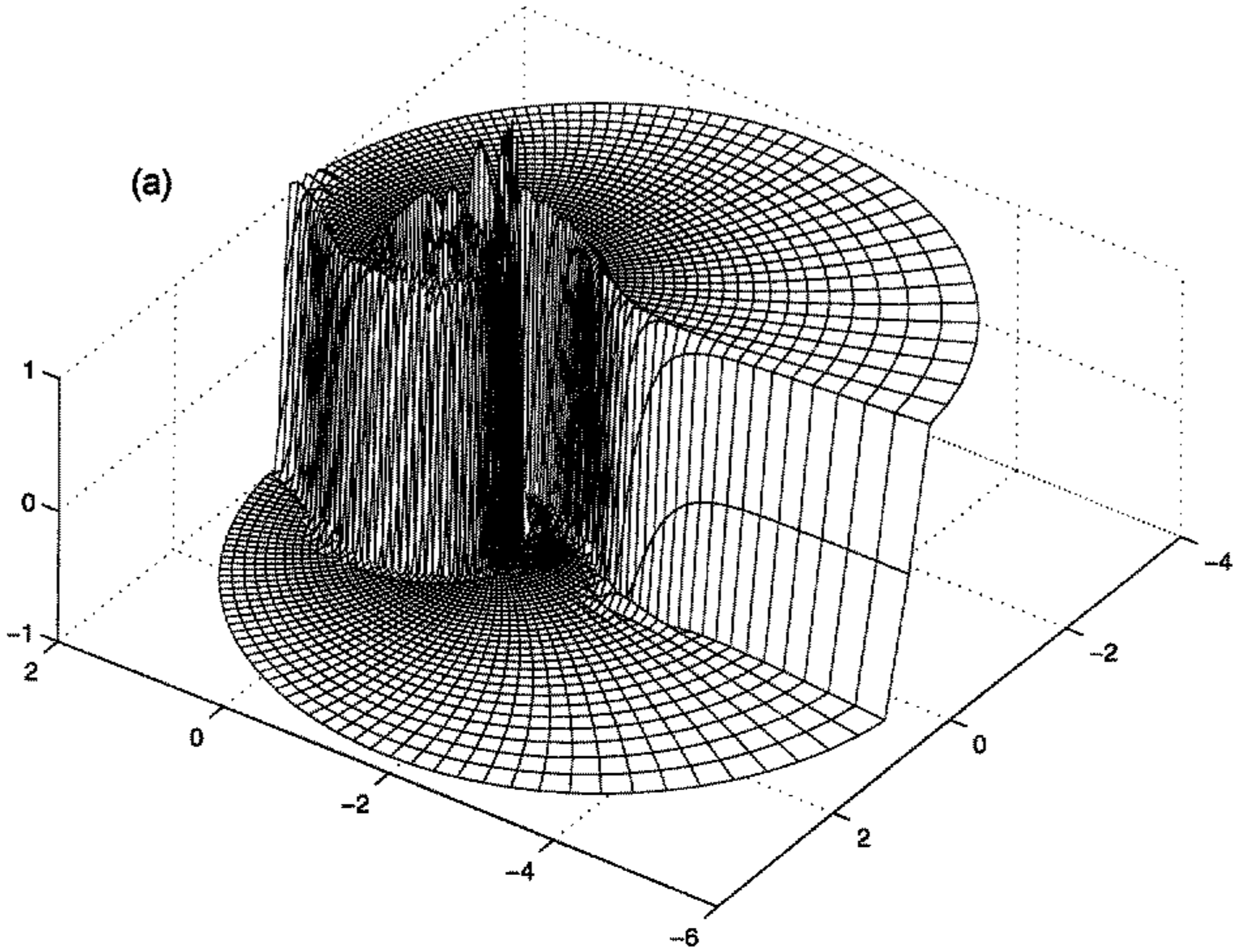

Figure 7. The numerical solution at $t = 2.5$, projected onto the plane tangent to the vortex centre, and obtained using cascade cubic-spline interpolation, with exact trajectories, without a monotonic filter, and with (a) 16 time-steps and (b) 64 time-steps.

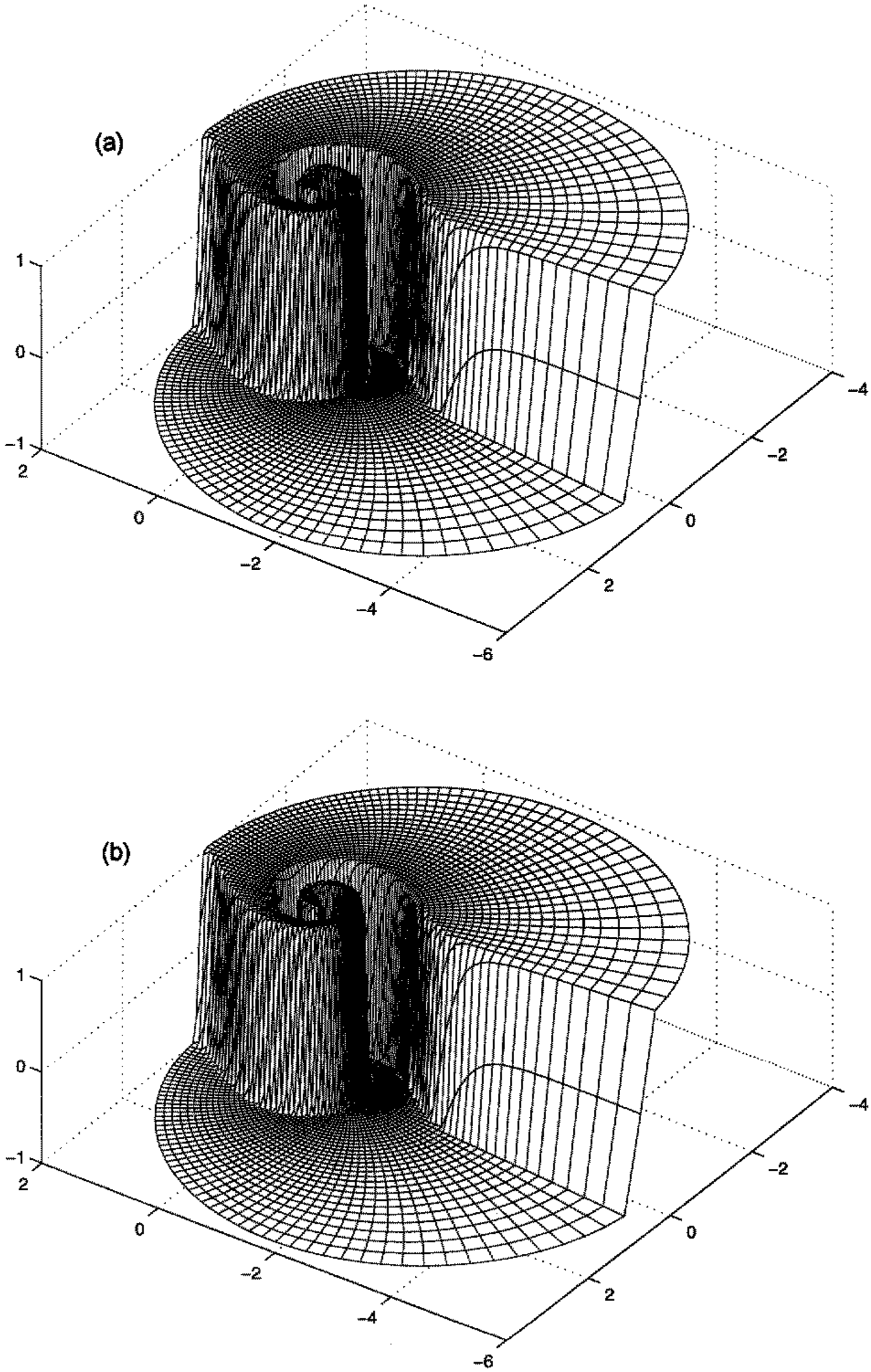

Figure 8. As in Fig. 7, but with the NCS99 monotonic filter.

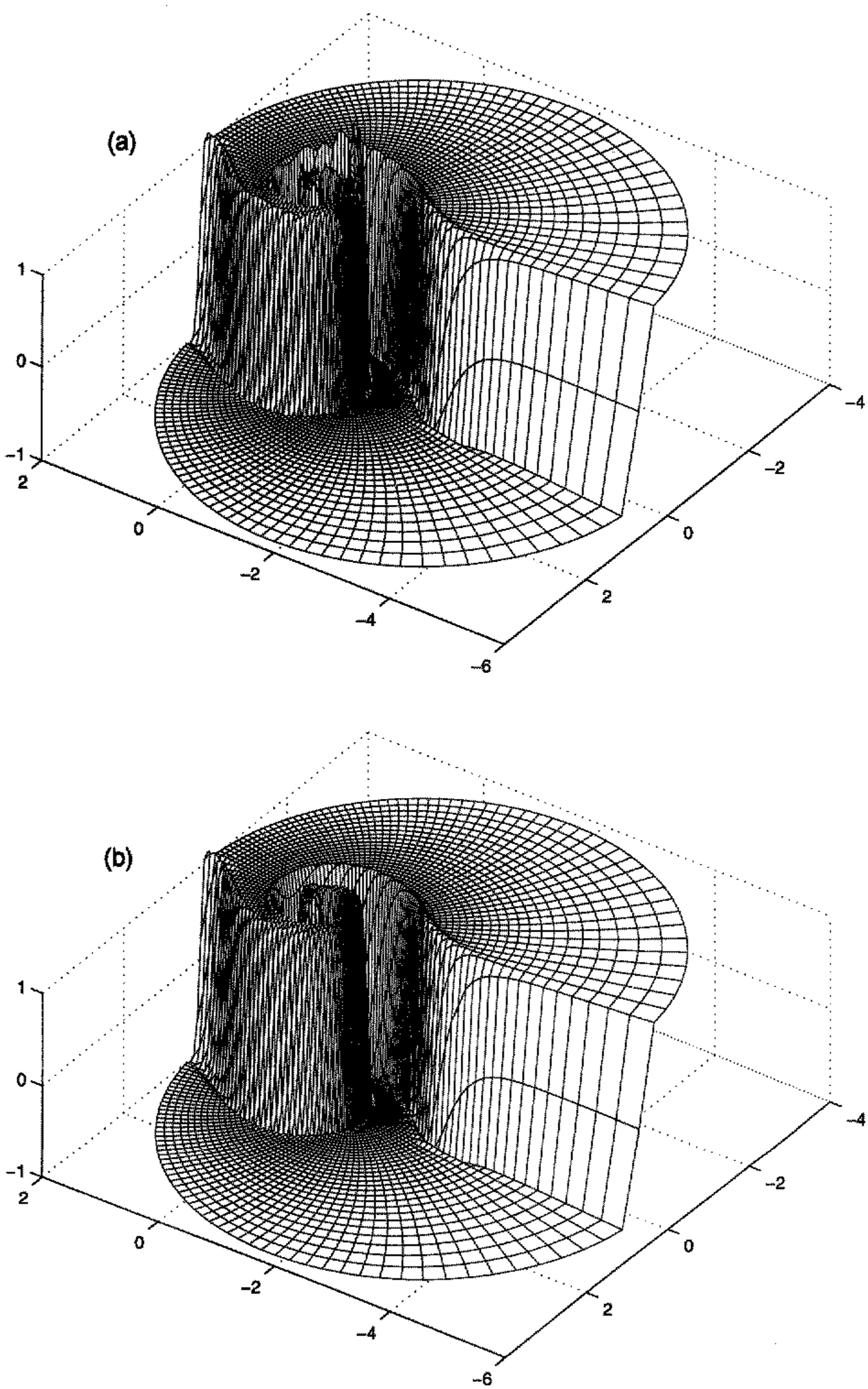

Figure 9. As in Fig. 7, but using cascade cubic-Lagrange interpolation.

TABLE 8. AS IN TABLE 6, BUT FOR CASCADE CUBIC-LAGRANGE INTERPOLATION

Monotonic filter	No. of *t*-steps	l_1	l_2	l_∞	*Mass*	V	ψ_{max}	ψ_{min}
No	16	0.0323	0.0994	1.5964	1.0044	−0.1005	0.4169	−0.1980
No	64	0.0384	0.1068	1.0126	1.0042	−0.1077	0.1296	−0.1168
Yes	16	0.0322	0.1063	1.5120	1.0038	−0.1224	0	0
Yes	64	0.0393	0.1190	1.0041	1.0061	−0.1361	0	0

5. CONCLUSION

An accurate and efficient cascade interpolator, previously proposed by the authors for semi-Lagrangian advection in Cartesian geometry, has been extended to spherical geometry. It has been evaluated using backward trajectories for two test problems—solid-body rotation and strong deformational flow—and found to be both accurate and efficient. The first problem is the widely used solid-body rotation of a cosine bell. The second is a generalization to spherical geometry of Doswell's idealized cyclogenesis problem with an exact solution, and its highly-deformational flow field is more challenging than solid-body rotation.

Three different interpolators have been used: cascade cubic-spline; cascade cubic-Lagrange; and bicubic-Lagrange. The monotonicity constraint of NCS99 has been applied for the deformational flow problem. Trajectories have been either evaluated exactly or approximately using the Côté and Staniforth (1988) algorithm with bilinear interpolation.

For the smooth solid-body rotation problem, using a 1-D cubic-spline interpolator instead of a 1-D cubic-Lagrange one in the cascade interpolation procedure virtually eliminates the stretching of the cosine bell in the direction of the flow. In particular the l_1, l_2 and l_∞ errors are all approximately four times smaller for cascade cubic-spline interpolation than for cascade cubic-Lagrange interpolation. Bicubic-Lagrange interpolation leads to marginally better results than does cascade cubic-Lagrange interpolation, but cascade cubic-spline interpolation leads to significantly better results than those obtained using either of these two Lagrange interpolators. Comparison of the described results with those of other studies show them to be very competitive.

For the more challenging deformational flow problem: overshoots and undershoots are noticeable in the integrations using the cascade cubic-spline interpolator without a monotonic filter, particularly for the longer time-step integrations; the monotonic NCS99 filter eliminates overshoots and undershoots while well maintaining the essential details of the exact solution; and the numerical solution is relatively insensitive to an increase of time-step. Using cascade cubic-Lagrange instead of cascade cubic-spline interpolation results in a less-severe Gibbs phenomenon in the absence of the monotonic NCS99 filter and the results of the two cascade interpolators are visually indistinguishable from one another when using the NCS99 filter.

The use of computed trajectories instead of exact ones has a marginal impact on the results for either of the two test problems.

How best to apply the cascade method to the interpolation of vector quantities in polar regions is still an open question. The applicability of the method to distributed-memory parallel-processing computers is also an open question. The cascade cubic-Lagrange interpolator would presumably be preferable to the cascade cubic-spline one, since the data and inter-processor communication are inherently more localized.

It is not clear (at least to us) how to apply the ideas outlined herein to efficiently perform cascade interpolation in the regions of reduced resolution around the two poles

using reduced-resolution Gaussian grids of the type discussed in Hortal and Simmons (1991) and Courtier and Naughton (1994). The proposed cascade algorithm could in principle be applied everywhere outside the two polar caps. However, as pointed out by one of the referees, this approach would be of limited applicability—for the grid used at ECMWF, this region is already restricted to within 25° of the equator at T213 resolution, and this shrinks to plus or minus 15° when using their experimental T639 resolution model with a 'linear' grid.

ACKNOWLEDGEMENTS

The preparation of schematic figures by Yves Chartier, Monique Tanguay's careful review of a first draft of the paper, and the helpful comments of three anonymous referees, are all gratefully acknowledged. The first author thanks the Natural Sciences and Engineering Research Council for providing a visiting fellowship.

APPENDIX

IDEALIZED CYCLOGENESIS IN SPHERICAL GEOMETRY—FURTHER DETAILS

The polar-stereographic tangent plane

Let (λ', θ') be a rotated coordinate system with north pole at (λ_0, θ_0) with respect to the original spherical coordinate system (λ, θ). Now define a plane tangent to the north pole of this rotated coordinate system. The coordinates on this tangent plane of a point that has been polar-stereographically projected from the arbitrary location (λ', θ') on the unit sphere are

$$X = m(\theta') \cos\theta' \cos\lambda', \tag{A.1}$$

$$Y = m(\theta') \cos\theta' \sin\lambda', \tag{A.2}$$

where

$$m(\theta') \equiv \frac{1 + \sin(\pi/2)}{1 + \sin\theta'} = \frac{2}{1 + \sin\theta'} \tag{A.3}$$

is the map-scale factor of this conformal polar-stereographic transformation, which is true at 90° N. The distance ρ of a point lying in this tangent plane from its contact point with the sphere is thus

$$\rho = (X^2 + Y^2)^{1/2} = m(\theta') \cos\theta' = \frac{2\cos\theta'}{1 + \sin\theta'}. \tag{A.4}$$

The variable ρ can be interpreted as being one of the two independent variables of a polar-coordinate system (ρ, λ') lying within the tangent plane, whose origin is at the plane's contact point with the sphere.

Maximum tangential velocity

Maximizing the expression given in (25), the maximum value of $u'(\theta')$occurs where

$$\tanh(\gamma\rho) = 1/\sqrt{3}, \tag{A.5}$$

i.e. where

$$\rho(\theta') = \frac{2\cos\theta'}{1+\sin\theta'} = \frac{1}{2\gamma}\ln\left(\frac{\sqrt{3}+1}{\sqrt{3}-1}\right). \tag{A.6}$$

Substituting (A.5) into (25) verifies that the maximum value of $u'(\theta')$ is unity. By expressing $\cos\theta'$ and $\sin\theta'$ in terms of $\tan(\theta'/2)$, (A.6) can be solved to yield

$$\theta' = 2\tan^{-1}\left(\frac{\gamma - c}{\gamma + c}\right), \tag{A.7}$$

where

$$c = \frac{1}{4}\ln\left(\frac{\sqrt{3}+1}{\sqrt{3}-1}\right) \approx 0.3292395. \tag{A.8}$$

Exact upstream particle positions

Analytically integrating (25) and $v' \equiv \mathrm{d}\theta'/\mathrm{d}t = 0$ backwards in time, the exact upstream position of a particle at time t that arrives at a point (λ', θ') at time $t + \Delta t$ is given by

$$\lambda'(t) = \lambda'(t + \Delta t) - \omega(\theta')\Delta t, \tag{A.9}$$

$$\theta' = \theta'(t + \Delta t). \tag{A.10}$$

Specifying the problem in the unrotated coordinate system

To specify the problem equivalently in the unrotated coordinate system (λ, θ), the following relations between the (λ', θ') and (λ, θ) coordinate systems are used (Ritchie 1987; McDonald and Bates 1989):

$$\lambda'(\lambda, \theta) = \tan^{-1}\left\{\frac{\sin(\lambda - \lambda_0)}{\sin\theta_0\cos(\lambda - \lambda_0) - \cos\theta_0\tan\theta}\right\}, \tag{A.11}$$

$$\theta'(\lambda, \theta) = \sin^{-1}\left\{\sin\theta\sin\theta_0 + \cos\theta\cos\theta_0\cos(\lambda - \lambda_0)\right\}, \tag{A.12}$$

$$\sin\theta = \sin\theta'\sin\theta_0 - \cos\theta'\cos\theta_0\cos\lambda', \tag{A.13}$$

$$\cos\theta\sin(\lambda - \lambda_0) = \cos\theta'\sin\lambda'. \tag{A.14}$$

Given the coordinates of a point in the unrotated coordinate system (λ, θ), the first two of these give the corresponding coordinates in the rotated coordinate system (λ', θ'). Taking the total derivative of the third, using (A.14) and the definition of velocity components, and noting that $v' \equiv \mathrm{d}\theta'/\mathrm{d}t = 0$ for the vortex, gives

$$v \equiv \frac{\mathrm{d}\theta}{\mathrm{d}t} = \omega(\theta')\cos\theta_0\sin(\lambda - \lambda_0), \tag{A.15}$$

where $\omega(\theta')$ is defined by (30). Similarly, differentiating (A.12) and using (A.15) gives

$$u \equiv \cos\theta\frac{\mathrm{d}\lambda}{\mathrm{d}t} = \omega(\theta')\left\{\sin\theta_0\cos\theta - \cos\theta_0\cos(\lambda - \lambda_0)\sin\theta\right\}. \tag{A.16}$$

Summarizing, to obtain u, v and ψ at a point (λ, θ) on the unrotated mesh:

- Compute the corresponding coordinates in the (λ', θ') system using (A.11)–(A.12).
- Compute v and u from (A.15)–(A.16), where $\omega(\theta')$ is defined by (30).
- Compute ψ from (29), where $\rho(\theta')$ and $\omega(\theta')$ are defined by (26) and (30).

REFERENCES

Bermejo, R. and Staniforth, A. 1992 The conversion of semi-Lagrangian advection schemes to quasi-monotone schemes. *Mon. Weather Rev.*, **120,** 2622–2632

Côté, J. and Staniforth, A. 1988 A two-time-level semi-Lagrangian semi-implicit scheme for spectral models. *Mon. Weather Rev.*, **116,** 2003–2012

Courtier, P. and Naughton, M. 1994 A pole problem in the reduced Gaussian grid. *Q. J. R. Meteorol. Soc.*, **120,** 1389–1407

Doswell, C. A. 1984 A kinematic analysis of frontogenesis associated with a nondivergent vortex. *J. Atmos. Sci.*, **41,** 1242–1248

European Centre for Medium-Range Weather Forecasts 1996 Proceedings of ECMWF Workshop on Semi-Lagrangian Methods. Available from European Centre for Medium-range Weather Forecasts, Shinfield Park, Reading RG2 9AX, UK

Hólm, E. V. 1995 A fully two-dimensional, nonoscillatory advection scheme for momentum and scalar transport equations. *Mon. Weather Rev.*, **123,** 536–552

Hortal, M. and Simmons, A. J. 1991 Use of reduced Gaussian grids in spectral models. *Mon. Weather Rev.*, **119,** 1057–1074

Leslie, L. M. and Purser, R. J. 1995 Three-dimensional mass-conserving semi-Lagrangian schemes employing forward trajectories. *Mon. Weather Rev.*, **123,** 2551–2566

Li, Y. and Chang, J. S. 1996 A mass-conservative, positive-definite, and efficient Eulerian advection scheme in spherical geometry and on a nonuniform grid system. *J. Appl. Meteorol.*, **35,** 1897–1913

Lin, S.-J. and Rood, R. B. 1996 Multidimensional flux-form semi-Lagrangian transport schemes. *Mon. Weather Rev.*, **124,** 2046–2070

McDonald, A. and Bates, J. R. 1989 Semi-Lagrangian integration of a gridpoint shallow water model on the sphere. *Mon. Weather Rev.*, **117,** 130–137

McGregor, J. L. 1996 Semi-Lagrangian advection on conformal-cubic grids. *Mon. Weather Rev.*, **124,** 1311–1322

Makar, P. A. and Karpick, S. R. 1996 Basis-spline interpolation on the sphere: applications to semi-Lagrangian advection. *Mon. Weather Rev.*, **124,** 182–199

Nair, R., Côté, J. and Staniforth, A. 1999 Monotonic cascade interpolation for semi-Lagrangian advection. *Q. J. R. Meteorol. Soc.*, **125,** 197–212

Priestley, A. 1993 A quasi-conservative version of the semi-Lagrangian advection scheme. *Mon. Weather Rev.*, **121,** 621–629

Purser, R. J. and Leslie, L. M. 1991 An efficient interpolation procedure for high-order three-dimensional semi-Lagrangian models. *Mon. Weather Rev.*, **119,** 2492–2498

1994 An efficient semi-Lagrangian scheme using third-order semi-implicit time integration and forward trajectories. *Mon. Weather Rev.*, **122,** 745–756

1996a Generalized Adams–Bashforth time integration schemes for a semi-Lagrangian model employing the second-derivative form of the horizontal momentum equation. *Q. J. R. Meteorol. Soc.*, **122,** 737–763

1996b 'High-order time integration and conservation in semi-Lagrangian models'. Pp. 6B.2–6B.3 in Preprints of 11th AMS Conference on NWP, Norfolk, VA. American Meteorological Society, Boston, MA

1997 High-order generalized Lorenz *N*-cycle schemes for semi-Lagrangian models employing second derivatives. *Mon. Weather Rev.*, **125,** 1261–1276

Rančić, M. 1992 Semi-Lagrangian piecewise biparabolic scheme for two-dimensional horizontal advection of a passive scalar. *Mon. Weather Rev.*, **120,** 1394–1406

Rasch, P. J. 1994 Conservative shape-preserving two-dimensional transport on a spherical reduced grid. *Mon. Weather Rev.*, **122,** 1337–1350

Ritchie, H. 1987 Semi-Lagrangian advection on a Gaussian grid. *Mon. Weather Rev.*, **115,** 608–619

Sun, W.-Y. and Yeh, K.-S. 1997 A general semi-Lagrangian advection scheme employing forward trajectories. *Q. J. R. Meteorol. Soc.*, **123,** 2463–2476

Sun, W.-Y., Yeh, K.-S. and Sun, R.-Y. 1996 A simple semi-Lagrangian scheme for advection equations. *Q. J. R. Meteorol. Soc.*, **122,** 1211–1226

Tolstykh, M. A. 1996 The response of a variable-resolution semi-Lagrangian NWP model to changes in horizontal interpolation. *Q. J. R. Meteorol. Soc.*, **122,** 765–778

Williamson, D. L. and Rasch, P. 1989 Two-dimensional semi-Lagrangian transport with shape-preserving interpolation. *Mon. Weather Rev.*, **117,** 102–129

Williamson, D. L., Drake, J. B., Hack, J. J., Jakob, R. and Swartztrauber, P. N. 1992 A standard test set for numerical approximations to the shallow water equations in spherical geometry. *J. Comput. Phys.*, **102,** 211–224